Abu Nasar Ghazali* and Srikanta Pal

Planar UWB Filter with Multiple Notched Band and Stopband with Improved Rejection Level

Abstract: Analysis and realization of a microstrip-based planar ultra-wideband (UWB) filter with integrated multiple notch elimination property and simultaneously extended upper stopband is proposed. Initially, a UWB filter based on back-to-back microstrip-to-CPW technology is designed. Later, multiple spiral defected ground structures (DGS) are embedded to obtain multiple passband notches. Further, double equilateral U (DEU)-type DGS are used to improve upon the rejection level in upper stopband. The multiple passband notches are results of embedded spiral-shaped DGS (SDGS), while extended upper stopband is the outcome of suppressed higher-order spurious harmonics. The flexible dual-attenuation poles of DEU-shaped DGS suppress the stopband harmonics and widen the stopband. An approximate lumped equivalent circuit model of the proposed filter is modelled. The filter is compact and its layout measures 25.26 mm $\times$ 11.01 mm. The measured result is in good agreement with the full-wave electromagnetic (EM) simulation and circuit simulation.

Keywords: double equilateral-U (DEU), extended stopband, microstrip filter, microstrip-to-CPW, spiral defected ground structure (SDGS), ultra-wideband (UWB)

DOI 10.1515/freq-2014-0194
Received October 23, 2014

1 Introduction

The emission mask (–75 mW/MHz) imposed by the Federal Communications Commission (FCC) on ultra-wideband (UWB) systems prevents them from being source of interference to other in-band wireless services [1]. However, these in-band radio services like WLAN, C band, X band, etc. being high-energy transmitters at their frequency of operation act as intentional radiators, thereby causing significant interference to the UWB systems. In order to circumvent this problem UWB filters with integrated band notch property became necessary. Necessity invoked exhaustive amount of research and development in the design and modelling of UWB filters with interference proof property [2]–[7].

Single narrow notched band is created by embedding parasitic coupled line to the UWB bandpass filter (BPF) [2] and by loading the input feed-lines with stepped impedance microstrip stub [3]. The notch in [2] is function of parasitic coupled line dimensions, whereas stepped impedance microstrip stub introduces its first transmission zero at 5.5 GHz in [3]. UWB filter with dual notch bands using asymmetric coupling strip is reported in [4] and a simplified composite right/left-handed (SCRLH) resonator-based UWB filter generates dual notches in [5]. The structure in [4] provides multiple paths for signal flow, which enables it to generate multiple transmission zeroes, whereas the SCRLH is equivalent to two shunt-connected series LC resonance circuit which generates the dual notch. A dual notched band UWB filter with two electromagnetic bandgap (EBG) structure is reported in [6]. A UWB filter with triple notched band using triple mode stepped impedance resonator is reported in [7]. Here the triple mode resonator is equivalent to three shunt-connected series LC resonance circuit which generates the triple notch. Another triple notched band UWB filter on an E-shaped multiple mode resonator (MMR) with three parallel U-shaped defected microstrip slots is reported in [8]. However, none of the above shows significant stopband extension.

Here we propose a microstrip-based UWB filter with triple notched band and simultaneously extended upper stopband. In this research we have chosen the back-to-back microstrip-to-CPW [9]-based UWB filter because of its inherent strong coupling, smooth passband response and good selectivity. Later, multiple defected ground structures (DGS) are embedded to the UWB filter so as to obtain triple passband notch and simultaneously extended upper stopband. Spiral-shaped DGS (SDGS) generate the passband notch. The notch frequency position is function of SDGS profile dimension, whereas notch bandwidth and notch number are related to SDGS cascading. Extended stopband is obtained by suppressing

***Corresponding author: Abu Nasar Ghazali,** Department of Electronics and Communication Engineering, BIT Mesra, Patna Campus, Patna 800014, India, E-mail: anghazali@gmail.com
Srikanta Pal, Department of Electrical Engineering, Shiv Nadar University, Gautam Buddha Nagar, Uttar Pradesh – 201314, India, E-mail: pal_srikanta@yahoo.co.uk

the spurious harmonics using the dual flexible attenuation poles of the double equilateral-U (DEU)-shaped DGS [10]. The proposed UWB filter is designed using the commercial, full-wave electromagnetic (EM) simulation software, IE3D, and is fabricated on substrate RT/Duroid 6010 of dielectric constant 10.8 and height 0.635 mm.

2 Design of UWB filter

The design methodology of the proposed filter is based on back-to-back microstrip-to-CPW technique [9], wherein the microstrip lines on the top are coupled to the CPW-based MMR on the ground via a common dielectric layer, as shown in Figure 1. The open circuited MMR, shown in Figure 2(a), has wide and narrow arms of impedance Z_1, Z_2 and corresponding electrical length $2\theta_1$, θ_2, respectively. In order to cover the entire UWB band, three quasi-equally spaced resonant frequencies, namely, at 4, 6.55 and 9 GHz, respectively, are selected. The electrical lengths θ_1 and θ_2 are then calculated from the admittance function of the MMR structure at resonance. In this case the optimized values obtained are Z_1 = 19 Ω, Z_2 = 38 Ω and θ_1 = 117°, θ_2 = 78°. The equivalent transmission line topology of this MMR consists of three cascaded sections as depicted in Figure 2(b).

For a general transmission line of electrical length θ, characteristic admittance Y_0 and terminated with load admittance Y_L, the input admittance Y_{in} at the left end looking into the right is given by [11]:

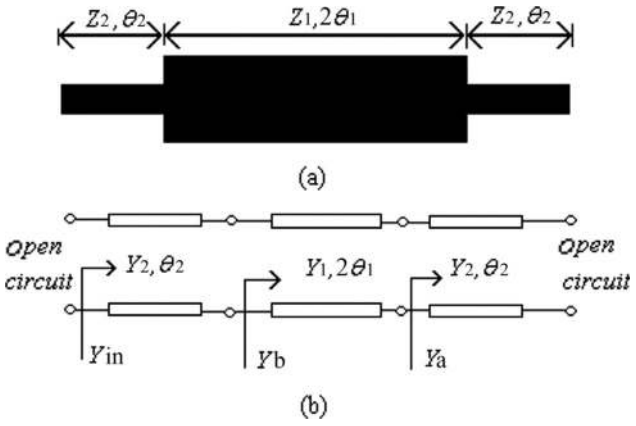

Figure 2: (a) Topology of the MMR for the proposed filter. Wide arm of characteristic impedance and electrical length Z_1 = 19 Ω and θ_1 = 117°, respectively, while narrow arm has characteristic impedance and electrical length Z_2 = 38 Ω and, θ_2 = 78°, respectively.
(b) Equivalent transmission line model of the MMR.

$$Y_{in} = Y_0\left(\frac{Y_L + jY_0 \tan\ \theta}{Y_0 + jY_L \tan\ \theta}\right) \tag{1}$$

When the load is open circuited, i.e. Y_L = 0, eq. (1) reduces to

$$Y_{in} = jY_0 \tan\theta \tag{2}$$

From Figure 2(b), the admittance Y_a can hence be written as

$$Y_a = jY_2 \tan\ \theta_2 \tag{3}$$

Following eq. (1), admittance Y_b, at centre, can be written as,

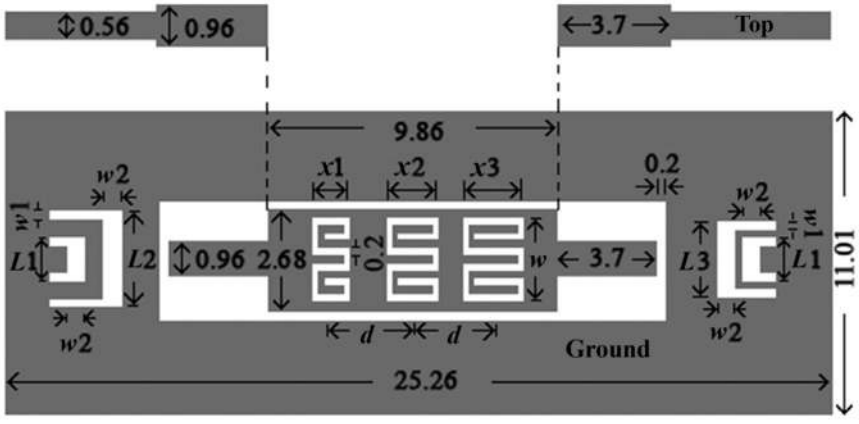

Figure 1: The proposed UWB filter. Microstrip lines on the top plane and ground plane at the bottom. The ground plane has three non-equidimensional SDGS units of equal width *w* and non-equidimensional lengths, *x*1, *x*2, *x*3, equally spaced distance *d* apart on the MMR. DEU-DGS [9] units at either ends are of variable lengths *L*1, *L*2 and *L*3 with equal horizontal and vertical widths *w*1 and *w*2, respectively. Dark shade is conductor and white shade etched part. All dimensions in mm.

$$Y_b = jY_1\left(\frac{\tan\theta_2 + R_z\tan 2\theta_1}{R_z - \tan 2\theta_1\tan\theta_2}\right) \quad (4)$$

where R_z is the ratio of two characteristic admittances corresponding to the two different width of the transmission line sections, i.e. $R_Z = Y_1/Y_2$.

Similarly Y_{in} can be written as:

$$Y_{in} = Y_2\left(\frac{Y_b + jY_2\tan\theta_2}{Y_2 + jY_b\tan\theta_2}\right) \quad (5)$$

$$= jY_2\left(\frac{R_z(\tan\theta_2 + R_z\tan 2\theta_1) + \tan\theta_2(Rz - \tan 2\theta 1\tan\theta_2)}{(R_z - \tan 2\theta_1\tan\theta_2) - R_z(\tan\theta_2 + R_z\tan 2\theta_1)\tan\theta_2}\right) \quad (6)$$

After simplification eq. (6) reduces to

$$Y_{in} = jY_2\frac{2(R_z\tan\theta_1 + \tan\theta_2)(R_z - \tan\theta_1\tan\theta_2)}{R_z(1-\tan^2\theta_1)(1-\tan^2\theta_2) - 2(1+R_z^2)\tan\theta_1\tan\theta_2} \quad (7)$$

At resonance $Y_{in} = 0$, therefore eq. (7) reduces to

$$R_z\tan\theta_1 + \tan\theta_2 = 0 \quad (8)$$

$$R_z - \tan\theta_1\tan\theta_2 = 0 \quad (9)$$

For the chosen MMR, $\theta_1 = 1.5.\theta_2$ and $\theta_2 = \theta$ (say), therefore eqs (8) and (9) reduce to

$$R_z\tan(1.5\theta) + \tan\theta = 0 \quad (10)$$

$$R_z - \tan(1.5\theta)\tan\theta = 0 \quad (11)$$

Solving the above equations using analytical method yields

$$\theta(f_1) = 2\tan^{-1}\left\{\frac{(4R_z+6) + \sqrt{(4R_z+6)^2 - 4R_z(3R_z+2)}}{2(3R_z+2)}\right\}^{1/2} \quad (12)$$

$$\theta(f_2) = 2\tan^{-1}\left\{\frac{(4R_z+6) + \sqrt{(4R_z+6)^2 - 4R_z(3R_z+2)}}{2R_z}\right\}^{1/2} \quad (13)$$

$$\theta(f_3) = 2\pi \quad (14)$$

The normalized frequencies are given by

$$\frac{f_2}{f_1} = \frac{2\tan^{-1}\left\{\frac{(4R_z+6) + \sqrt{(4R_z+6)^2 - 4R_z(3R_z+2)}}{2R_z}\right\}^{1/2}}{2\tan^{-1}\left\{\frac{(4R_z+6) + \sqrt{(4R_z+6)^2 - 4R_z(3R_z+2)}}{2(3R_z+2)}\right\}^{1/2}} \quad (15)$$

$$\frac{f_3}{f_1} = \frac{2\pi}{2\tan^{-1}\left\{\frac{(4R_z+6) + \sqrt{(4R_z+6)^2 - 4R_z(3R_z+2)}}{2(3R_z+2)}\right\}^{1/2}} \quad (16)$$

Figure 3(a) plots these normalized frequencies against R_z. It is observed from the figure that as R_z increases the first two resonances move close to each other and they are simultaneously excited to generate an UWB. Thus it can be inferred that the position of resonances and therefore the width of passband of UWB can be controlled by varying R_z.

For the chosen MMR a variable x is considered and is defined as

$$x = \frac{\theta_2}{\theta_2 + \theta_1} \quad (17)$$

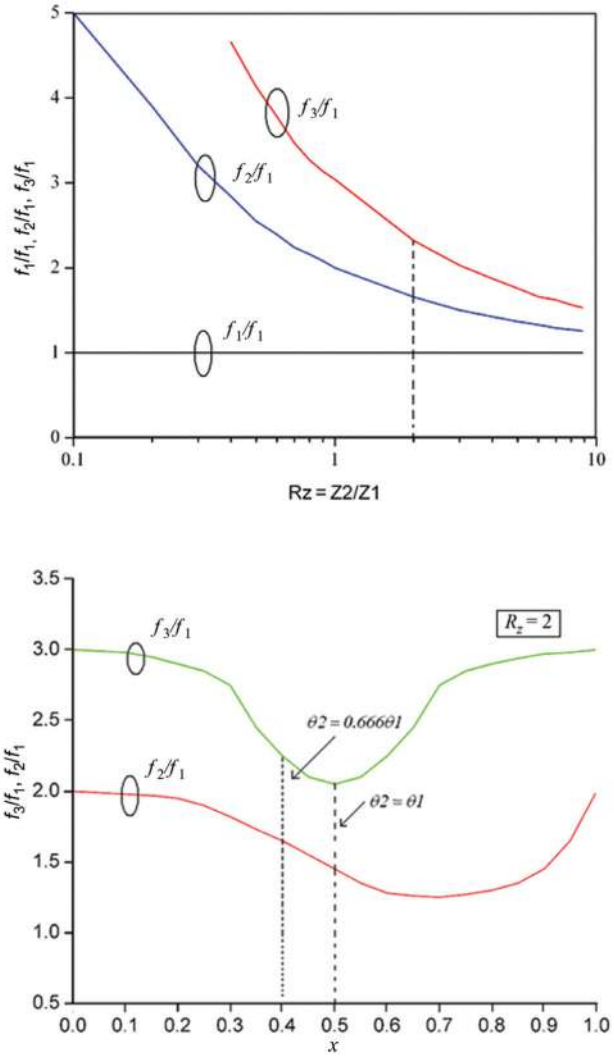

Figure 3: Resonant spectrum of only the MMR for (a) $\theta_1 = 1.5\theta_2$ and (b) $R_z = 2$.

Equations [10] and [11] can therefore be expressed as:

$$R_z \tan\theta_1 + \tan\frac{x}{1-x}\theta_1 = 0 \tag{18}$$

$$R_z - \tan\theta_1 \tan\frac{x}{1-x}\theta_1 = 0 \tag{19}$$

Solving eqs [18] and [19] provides us with odd and even mode resonant frequencies, 4, 6.55 and 9 GHz, respectively.

For the proposed UWB filter with $R_z = 2$, the normalized resonant frequencies are plotted against variable x, as shown in Figure 3(b). It is seen from Figure 3(b) that for $\theta_2 = 0.666\theta_1$ (i.e. $x = 0.4$), the three resonant frequencies (4, 6.55 and 9 GHz) are positioned reasonably close and approximately equidistant from each other. These resonant modes are then simultaneously excited so as to attain the requisite UWB passband in the proposed filter. The denominator of eq. (7) generates inband harmonics which when added up with the fundamental harmonics (zeroes of numerator of eq. (7)) produce the entire UWB band. Additionally, zeros of denominator obtained from eq. (21) depicts the presence of spurious harmonics in the upper stopband.

Having optimally modelled the MMR, the next step involves optimizing the microstrip-to-CPW transition. The transition consists of upper microstrip conductor electrically coupled to the MMR-based CPW via the common dielectric, as shown in Figure 4(a). The filter structure is symmetric. In the corresponding figure the left half of the coupling transition between the microstrip line on the top and the coplanar MMR on the bottom is only shown. This capacitive coupling is characterized by an equivalent unified J-inverter network [12] depicted in Figure 4(b). The J-inverter admittance represents the capacitive coupling extent. In order to achieve maximum coupling at the central UWB frequency, lengths of coupled lines are optimized close to $\lambda_g/4$. This tight EM coupling of the transition reduces the parasitic radiation loss [9]. The resonance response of the MMR alone can be achieved when there is no coupling present between the MMR in the ground plane and microstrip lines on top plane. This kind of coupling is referred here "weak coupling". To realize a practical UWB filter this MMR is required to be coupled strongly and efficiently to microstrip lines on the top plane. This sort of coupling is termed here as "tight coupling". The comparative frequency response for both the weak and tight coupling cases is displayed in Figure 4(c).

3 Notched band implementation

A controllable notch in passband, which is helpful in circumventing frequency selective in-band interference from other devices, is generated by implementing SDGS unit on the MMR. The resonant frequency of the notch is, $f_0 = 1/(2 \times \pi \times \sqrt{(L \times C)})$, where L and C are inductance and capacitance, respectively.

The dimensions of UWB filter designed in Section 2 are kept constant throughout the paper. The MMR with $Z_1 = 19\ \Omega$, $Z_2 = 38\ \Omega$ and $\theta_1 = 117°$, $\theta_2 = 78°$ has an SDGS unit of maximum possible width ($w = 2.3$ mm) and variable finger length x, implemented at its centre, as shown in the inset of Figure 5(a). Maximum width of SDGS is considered in order to achieve maximum controllability of the passband notch. The notch resonant frequency is function of finger length x. From Figure 5(a) it is seen that on increasing x value, the resonant frequency is lowered due to the increase in effective L and C.

The transmission phase characteristics (angle of S_{21}) of the UWB filter is shown in Figure 5(b). Compared to the UWB filter without SDGS unit, the SDGS etched filter response shows faster and slower phase variations below and above the notch resonant frequency [13].

The reason for this is when:

(1) $f < f_0$; $2\pi fL < 1/(2\pi fC)$, i.e. the inductive reactance is less than capacitive reactance and hence current traverses the path of less resistance around the SDGS leading to increase of effective inductance, thus leading to faster phase variation.
(2) For $f > f_0$; $2\pi fL > 1/(2\pi fC)$, i.e. the inductive reactance is more than capacitive reactance and hence current travelling the path of less resistance moves across the SDGS causing the charge to accumulate at the slots leading to increase of effective capacitance, which in turn leads to slower phase variation.
(3) And when $f = f_0$; $2\pi f_0 L = 1/(2\pi f_0 C)$, jumping occurs at resonance.

To increase the bandwidth of the notch, multiple equidimensional SDGS units are cascaded on the MMR. The increase in notch bandwidth is due to the increased EM coupling among the SDGS units when placed close to each other. Whereas increasing the distance between the SDGS units reduces the notch bandwidth due to weak EM coupling. Figure 6(a) depicts the notch bandwidth variation when three equidimensional SDGS units are placed equal distance d apart. Table 1 shows the comparative notch width variation due to d, for two and three equidimensional SDGS units on the MMR. Multiple passband interferences can be eliminated by embedding non-equidimensional SDGS units on the MMR.

Figure 6(b) depicts dual-controllable notches when two non-equidimensional SDGS units are cascaded on the

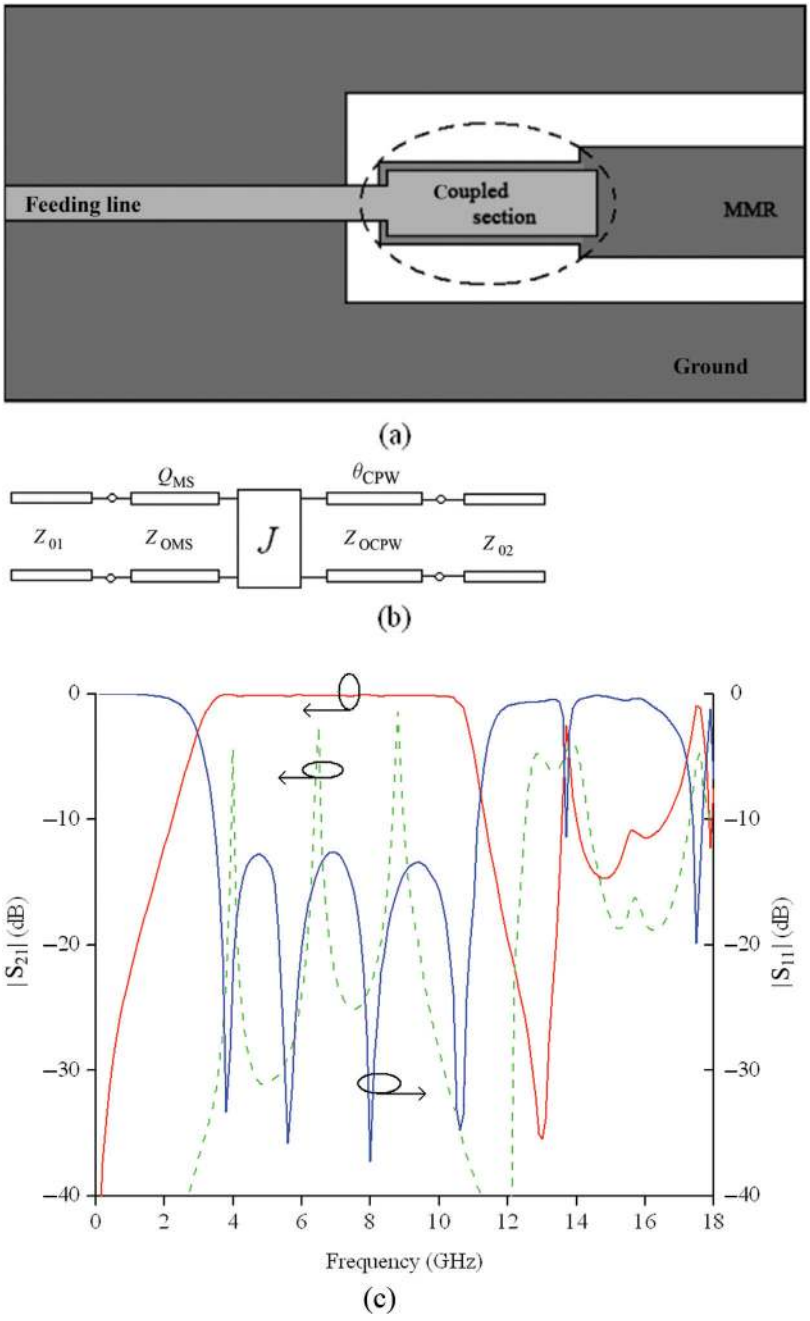

Figure 4: (a) Illustration of left half of the coupling transition between the microstrip line on the top and the coplanar MMR on the bottom. (b) Equivalent J-inverter network for the capacitive coupling transition. Z_{01} and Z_{02} are characteristic impedance of feeding lines. Z_{OMS} and Z_{OCPW} are characteristic impedances of microstrip line and CPW respectively. (c) Frequency response for weak and tight coupling.

MMR. Similarly, cascading three non-equidimensional SDGS units at equal distances generate controllable triple narrow notches as shown in Figure 6(c). It is seen from Figure 6(b) and (c) that on increasing the finger lengths the multiple notches move towards the lower end of UWB passband while reducing the finger length causes them to shift towards higher end of UWB spectrum.

4 Extended upper stopband

Presence of higher order stopband harmonics is one of the major disadvantages of MMR-based UWB filters. In order to extend the upper stopband attenuation poles need to be placed at these spurious harmonic points. In order to improve the stopband level and its width many

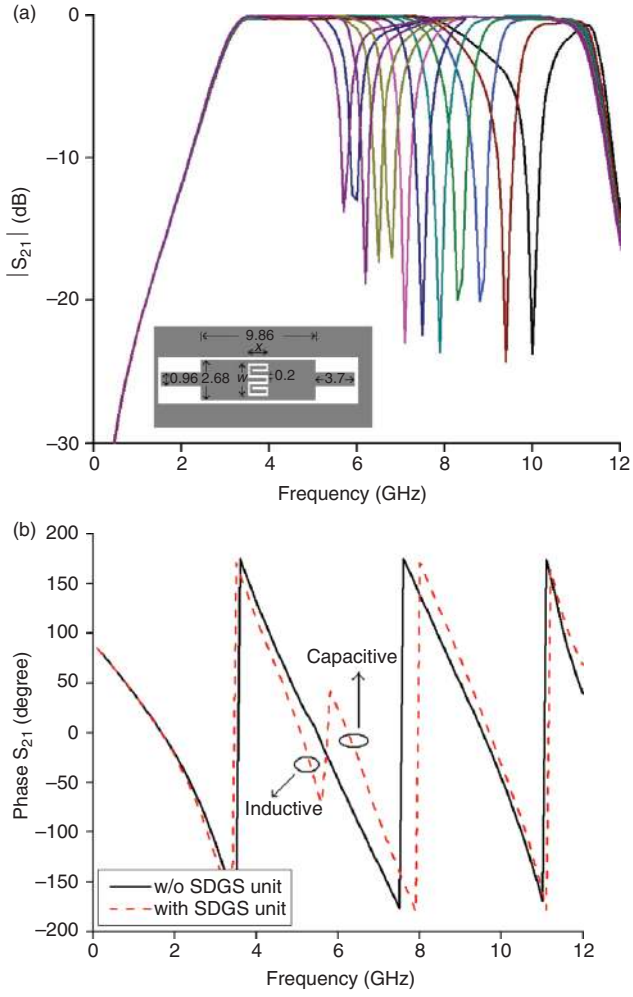

Figure 5: (a) Controllable notches for SDGS of width $w = 2.3$ mm and folded line length x. (b) Transmission phase characteristics for single SDGS unit of $w = x = 2.3$ mm.

types of DGSs are initially considered. A comparative result on performance of different DGSs found in Figure 5 of [10] is observed and DEU-DGS is chosen in this manuscript for its better rejection level and wider bandwidth [10]. Unlike the conventional DGSs, which generate single attenuation pole, the DEU-DGS unit generates dual flexible attenuation poles, thereby increasing the degree of freedom in design. Ting et al. [10] showed that DEU-DGS unit places two finite attenuation poles at two different frequencies, with almost no change in characteristics of other frequencies. Positioning of these poles is function of the DEU-DGS geometry.

In DEU-DGS [10], with slots vertical length ($L1$, $L2$) fixed, on increasing the horizontal section width of U slots ($w1$), both the attenuation poles are pulled to lower frequencies while both are shifted to higher frequencies when the width of the vertical sections of the U slots ($w2$) is increased. With widths ($w1$, $w2$) of U slot fixed, it is observed that the lower attenuation pole can be regulated by adjusting longer slot length $L2$ while higher pole can be regulated by adjusting shorter slot length $L1$.

The back-to-back microstrip-to-CPW-based UWB filter without DEU-DGS units depicts spurious harmonics at 13.89 and 17.7 GHz. The dimensional parameters of the DEU-DGS units are optimized to generate two attenuation poles at those spurious harmonics. The final optimized dimensions of the DEU-DGS: $w1 = 0.2$, $w2 = 0.5$, $L1 = 0.96$, $L2 = 2$ and $L3 = 1.6$ mm, respectively, when applied to the UWB filter structure suppresses the spurious harmonics and extends the stopband till 17.6 GHz with attenuation greater than −23 dB as shown in Figure 7(a).

Figure 7(b) depicts the presence of spurious harmonics at 13.8 and 17.4 GHz for the single notch structure. To suppress these harmonic points optimized DEU-DGS of dimensions $w1 = 0.2$, $w2 = 0.5$, $L1 = 0.96$, $L2 = 2$ and $L3 = 1.6$ mm, respectively, are implemented. It is observed from Figure 7(b) that the stopband extends up to 18 GHz with depth greater than −26 dB.

The dual notch structure displays presence of spurious harmonics at 13.4 and 17.5 GHz, as shown in Figure 7(c). With optimized DEU-DGS of dimensions $w1 = 0.2$, $w2 = 0.5$, $L1 = 0.96$, $L2 = 2.1$ and $L3 = 1.6$ mm, respectively, implemented, the stopband is found to suppress below −25 dB till 18 GHz causing minimum distortion to the dual passband notches.

The proposed triple notch structure is observed to possess spurious stopband harmonics at 13.4, 14.4 and 17.2 GHz, as depicted in Figure 7(d). To suppress these harmonic points DEU-DGS of dimensions $w1 = 0.2$, $w2 = 0.5$, $L1 = 0.96$, $L2 = 2.1$ and $L3 = 1.6$ mm, respectively, are implemented which suppress the stopband below −23 dB up to 18 GHz. Also observed is the minimum distortion to passband notches and other frequency characteristics.

5 Approximate equivalent circuit

In this section the development of approximate lumped equivalent circuit model for the back-to-back microstrip-to-CPW-based UWB filter as well as single, dual and triple notch structures are discussed. To approximate the lumped element equivalent circuit model of the UWB filter is complex due to frequency dependent substrate parameters and parasitic coupling.

The lumped equivalent circuit consists of basic block, namely MMR, whose lumped model is depicted

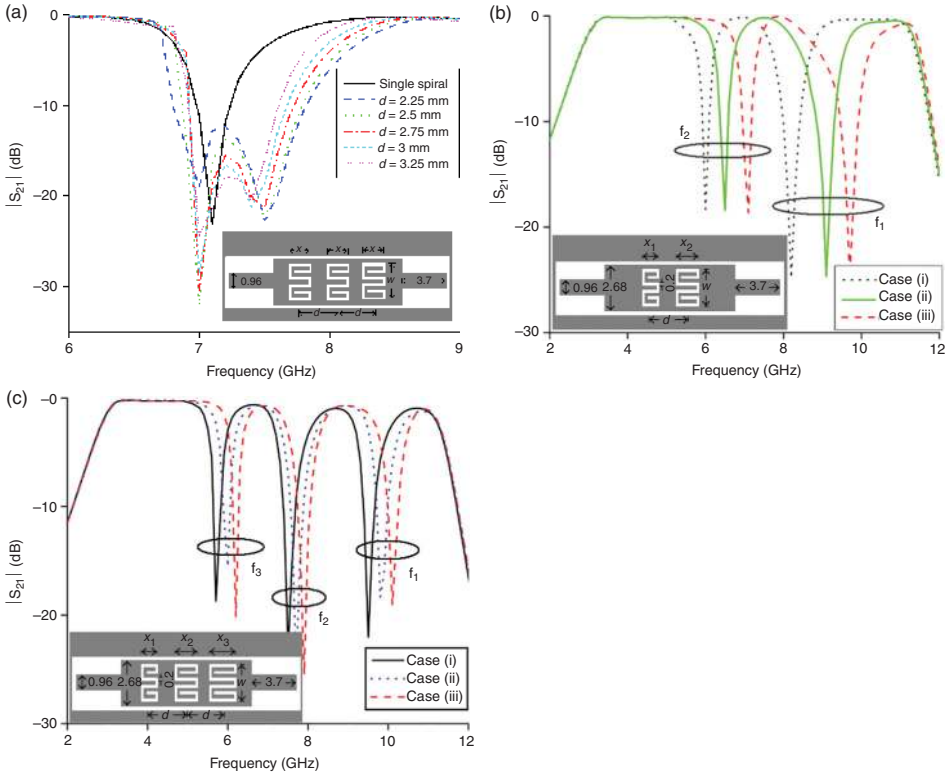

Figure 6: (a) Widened notches centred at 7.15 GHz for three equidimensional SDGS units of w = 2.3 mm and x = 1.8 mm placed equal distance d apart. (b) Controllable dual notches for three different cases with d = 3 mm. Case (i) x_1 = 1.6 mm and x_2 = 2.3 mm f_1 = 8.4 and f_2 = 5.7 GHz, respectively. Case (ii) x_1 = 1.4 mm and x_2 = 2.2 mm f_1 = 8.9 and f_2 = 6 GHz, respectively. Case (iii) x_1 = 1.3 mm and x_2 = 2.1 mm f_1 = 9.5 and f_2 = 6.2 GHz, respectively. (c) Controllable triple notches for three different cases with d = 3 mm. Case (i) x_1 = 1.3 mm, x_2 = 1.7 mm and x_3 = 2.3 mm, f_1 = 9.5, f_2 = 7.5 and f_3 = 5.7 GHz, respectively. Case (ii) x_1 = 1.25 mm, x_2 = 1.65 mm and x_3 = 2.2 mm, f_1 = 9.8, f_2 = 7.7 and f_3 = 6 GHz, respectively. Case (iii) x_1 = 1.2 mm, x_2 = 1.6 mm and x_3 = 2.1 mm, f_1 = 10.1, f_2 = 7.9 and f_3 = 6.2 GHz, respectively.

Table 1: Bandwidth (BW) of single SDGS unit = 0.19 GHz.

d (mm)	Two SDGS unit BW (GHz)	Three SDGS unit BW (GHz)
2.25	0.64	0.98
2.50	0.58	0.88
2.75	0.54	0.82
3.00	0.50	0.77
3.25	0.47	0.72

in Figure 8(a). The MMR controls the passband width and selectivity. MMR is constructed from inductances $L4$, $L5$, $L6$ and capacitance $C4$. The series resonator $L4$, $C4$ controls the higher passband roll-off, whereas $L6$ controls the lower passband selectivity. The passband smoothness is controlled by $L5$. The DEU-DGS units, with parallel resonant circuits of $L7$, $C7$ and $L8$, $C8$ as its equivalent model, are coupled to the MMR via the coupling capacitor Cc. The lumped elements are tuned to get circuit response matching closely with the full-wave EM simulation response. The optimized values obtained are $L4 = 1.87$ nH, $L5 = 1.16$ nH, $L6 = 4.11$ nH, $L7 = 0.074$ nH, $L8 = 0.0409$ nH, Cc = 0.7 pF, $C4 = 0.076$ pF, $C7 = 2.158$ pF, $C8 = 2.045$ pF. The comparative S parameter response for full-wave EM and circuit simulation is depicted in Figure 8(b).

Figure 8(c) presents the equivalent circuit model of the single notch structure. The SDGS is represented by a parallel resonator circuit with resonant notch frequency $f_0 = 1/2\pi\sqrt{(L_1C_1)}$. For the filter with notch frequency f_0 at 6 GHz, the optimized circuit model has parameter values, $L1 = 0.114$ nH, $L4 = 1.92$ nH, $L5 = 1.16$ nH, $L6 = 4.32$ nH, $L7 = 0.0789$ nH, $L8 = 0.0489$ nH, Cc = 0.69 pF, $C1 = 6.63$ pF, $C4 = 0.075$ pF, $C7 = 1.918$ pF, $C8 = 1.782$ pF. Figure 8(d) depicts the comparative full-wave EM and circuit-simulated S parameter response. The equivalent circuit model of the multinotch structure consists of resonant circuits coupled via T-network (Figure 8(c)) whose parameters (Ls and Cp) are from eq. (14) as:

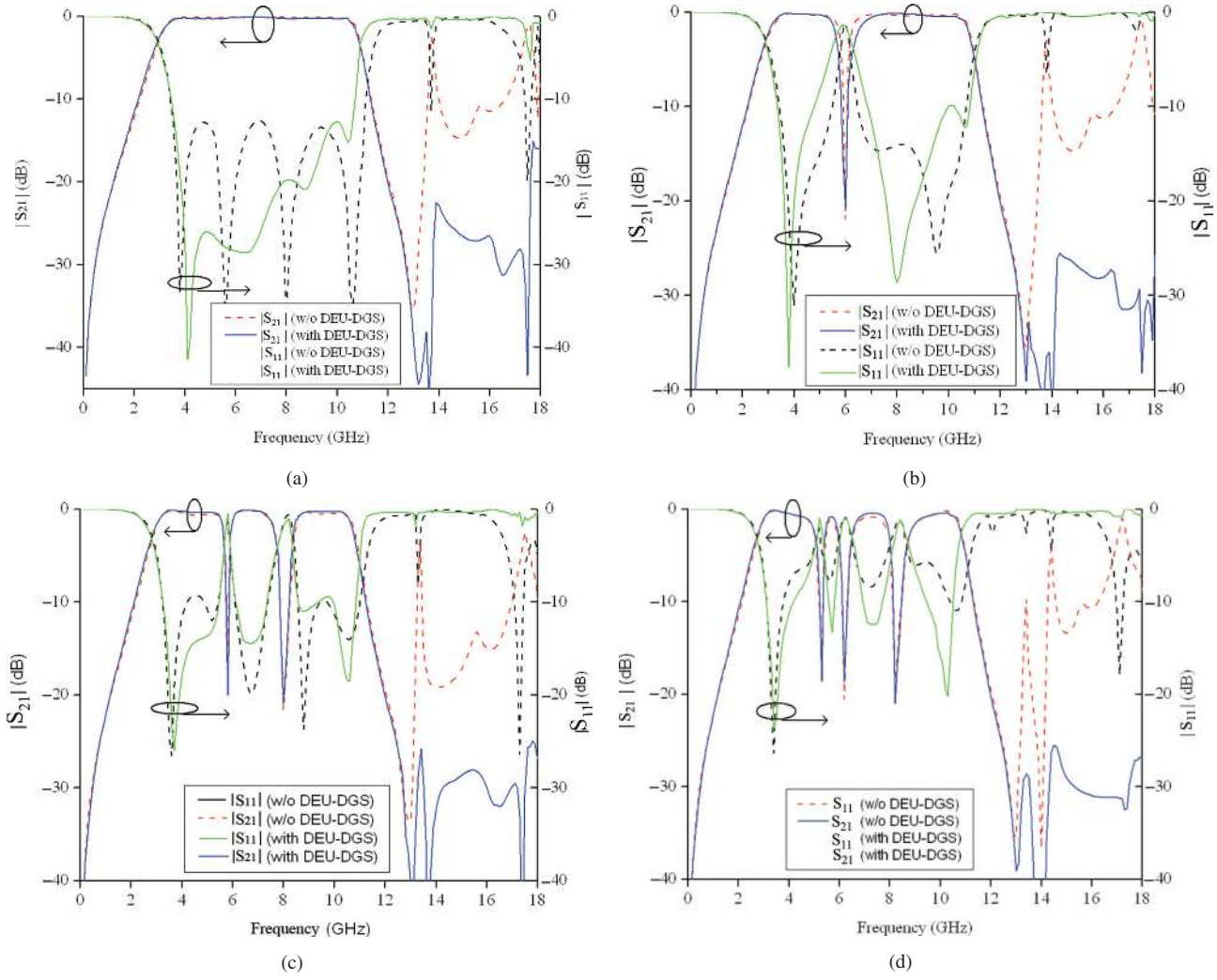

Figure 7: *S* parameter response with and without DEU-DGS for (a) without notch (b) single, (c) dual and (d) triple notch structures.

$$Cpi = -\frac{1}{2\pi f_{Ti} X(i+1), i}, i = 1, 2 \tag{20}$$

$$Lsi = \frac{Xii - X(i+1), i}{2\pi f_{Ti}} + \frac{Li}{\left(f_{Ti}/f_{0i}\right)^2 - 1}, i = 1, 2, 3, 4 \tag{21}$$

Where f_T is the transit frequency between resonant notch frequencies f_{oi} and X is the imaginary part of Z parameter at the transit frequency f_T.

The approximate equivalent circuit for the dual notch structure is shown in Figure 9(a). The extracted circuit parameters for notch frequencies f_{01} = 6 and f_{02} = 8.15 GHz are $L1$ = 0.114 nH, $L2$ = 0.2063 nH, $L4$ = 1.92 nH, $L5$ = 1.16 nH, $L6$ = 4.32 nH, $L7$ = 0.0789 nH, $L8$ = 0.0489 nH, $Ls1$ = 0.979 nH, $Ls2$ = −0.858 nH, Cc = 0.69 pF, $C1$ = 6.63 pF, $C2$ = 1.85 pF, $C4$ = 0.075 pF, $C7$ = 1.918 pF, $C8$ = 1.702 pF, $Cp1$ = 0.0133 pF. The negative value of inductance Ls2 is acceptable for circuit modelling as the case coincides with a lumped-element negative elements [14]. Figure 9(b) plots the comparative full-wave EM and circuit-simulated *S* parameter response.

The approximate equivalent circuit model of the proposed filter structure with triple notches at f_{01} = 5.2, f_{02} = 6.1 and f_{03} = 8.15 GHz, respectively, is shown in Figure 9 (c). The optimized circuit parameters obtained are $L1$ = 0.412 nH, $L2$ = 0.207 nH, $L3$ = 0.206 nH, $L4$ = 2 nH, $L5$ = 1.51 nH, $L6$ = 4.32 nH, $L7$ = 0.0408 nH, $L8$ = 0.0678 nH, $Ls1$ = 0.989 nH, $Ls2$ = −0.822 nH, $Ls3$ = 0.955 nH, $Ls4$ = −0.822 nH, Cc = 0.69 pF, $C1$ = 2.274 pF, $C2$ = 3.18 pF, $C3$ = 0.206 pF, $C4$ = 0.06805 pF, $C7$ = 2.448 pF, $C8$ = 2.15 pF, $Cp1$ = 0.00904 pF, $Cp2$ = 0.00648 pF. The comparative *S* parameter response of triple notch structure using full-wave EM and circuit simulation is as shown in Figure 9(d).

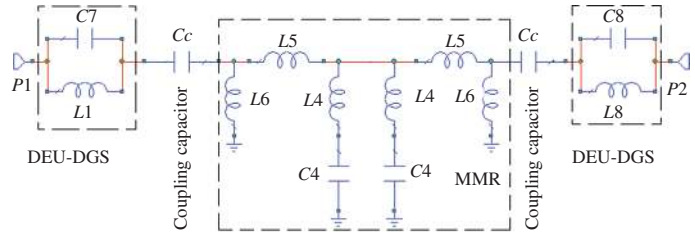

(a)

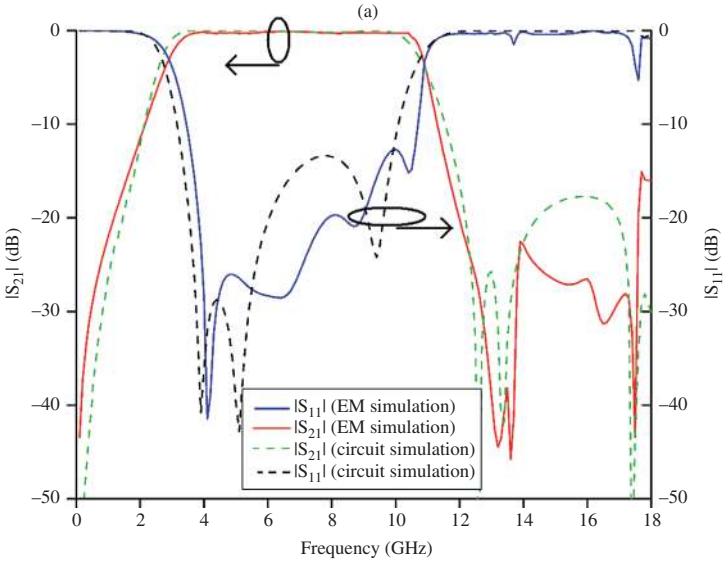

(b)

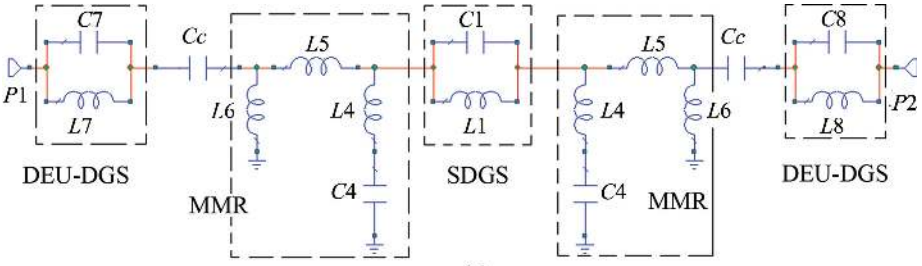

(c)

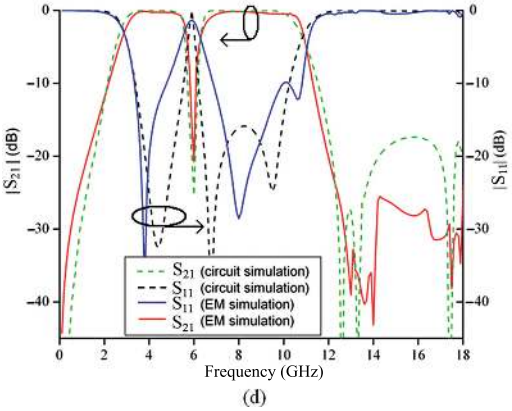

(d)

Figure 8: (a) Approximate lumped element equivalent circuit model of the microstrip-to-CPW-based UWB filter. (b) Comparative EM and circuit *S* parameter characteristics. (c) Approximate lumped element equivalent circuit model for the single notch structure. (d) Comparative full-wave EM and circuit-simulated frequency characteristics for the single notch structure.

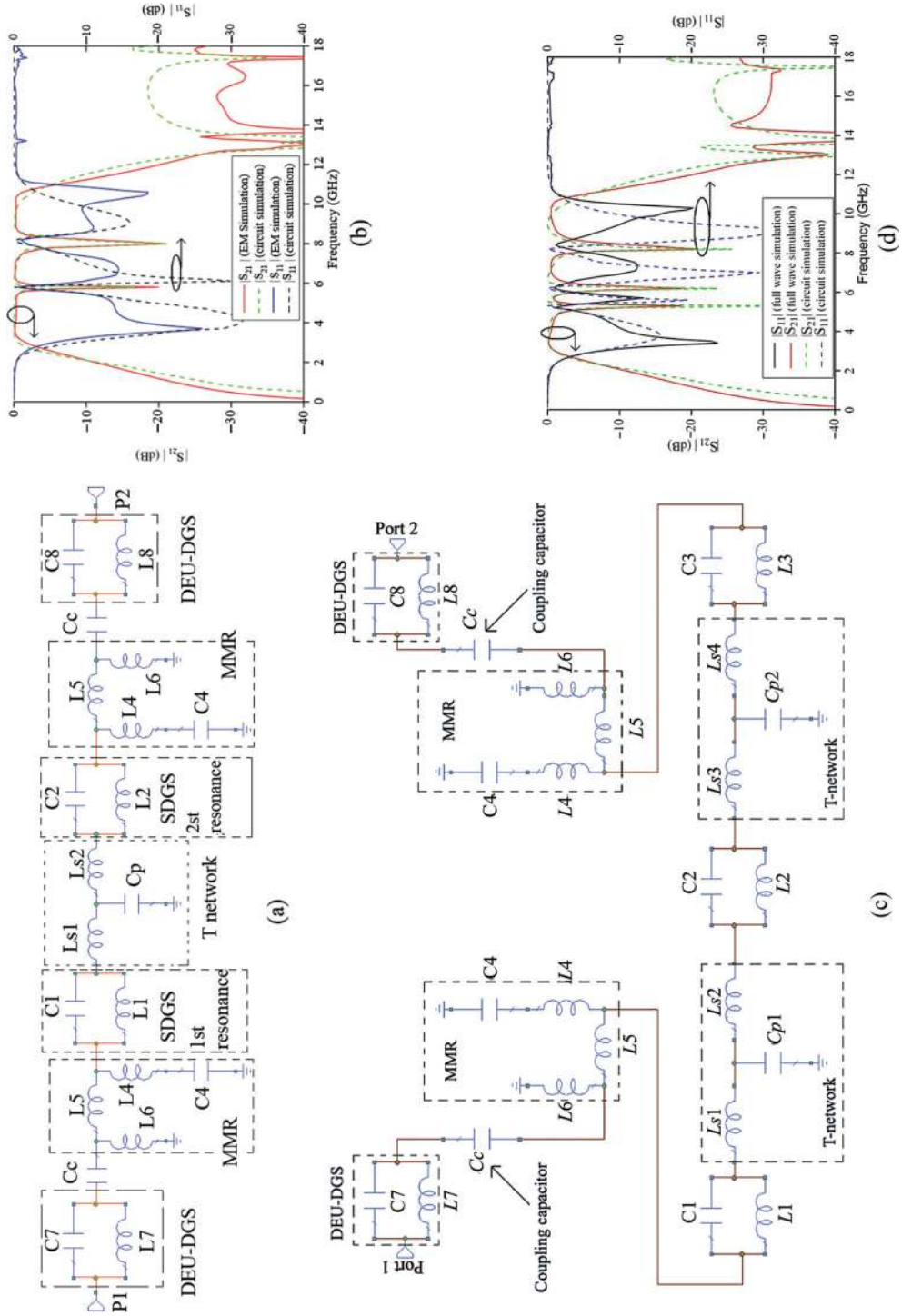

Figure 9: (a) Approximate lumped element equivalent circuit model for the dual notch structure. (b) Comparative full-wave EM and circuit-simulated frequency characteristics for the dual notch structure. (c) Approximate lumped element equivalent circuit model for the proposed triple notch structure. (d) Comparative full-wave EM and circuit-simulated frequency characteristics for the proposed triple notch structure.

The comparative S parameter response for all the structures show difference in S_{11} achieved by full-wave simulations and lumped model. Exact modelling of all the parasitic couplings in the lumped element equivalent model is a difficult task.

6 Measurement and results

The S parameter and group delay characteristics of the fabricated filter is measured using Agilent vector network analyser N5230A. The picture of the fabricated filter is shown in Figure 10(a). The comparative measured and simulated S parameter responses are shown in Figure 10(b) and (c). The passband observed is from 2.7 to 10.6 GHz while the upper stopband extends up to 18 GHz with rejection level greater than −26 dB. The return loss is under −11 dB throughout the passband. The maximum insertion loss observed in the passband is −0.3 dB before the first notch, −0.5 dB between first and second notch, −0.55 dB between second and third notch and −0.42 dB after the third notch. Three notched bands of 3 dB fractional bandwidth (FBW) 3.8%, 3.7%, 4.3%, respectively, and attenuation greater than −13 dB at the centre notch frequency is observed. The group delay measured is < 0.57 ns in 2–5 GHz, < 0.51 ns in 5.5–5.9 GHz, < 0.32 ns in 6.44–8 GHz and < 0.33 ns in 8.75–10.6 GHz band, as depicted in Figure 10(d). The discrepancy between measurements and simulations is mainly due to the fabrication error, finite substrate and reflection from connectors. The overall size of the proposed filter is 25.26 mm × 11.01 mm.

A comparative study of the proposed structure with other reported UWB filters with notched band and extended stopband is presented in Table 2. It is seen from Table 2 that the structure proposed in this manuscript is of smaller dimension compared to [3], [5]–[8]. Also the stopband response is wider and deeper compared to [3]–[8]. The above features make the filter a useful candidate for the present-day UWB communication systems.

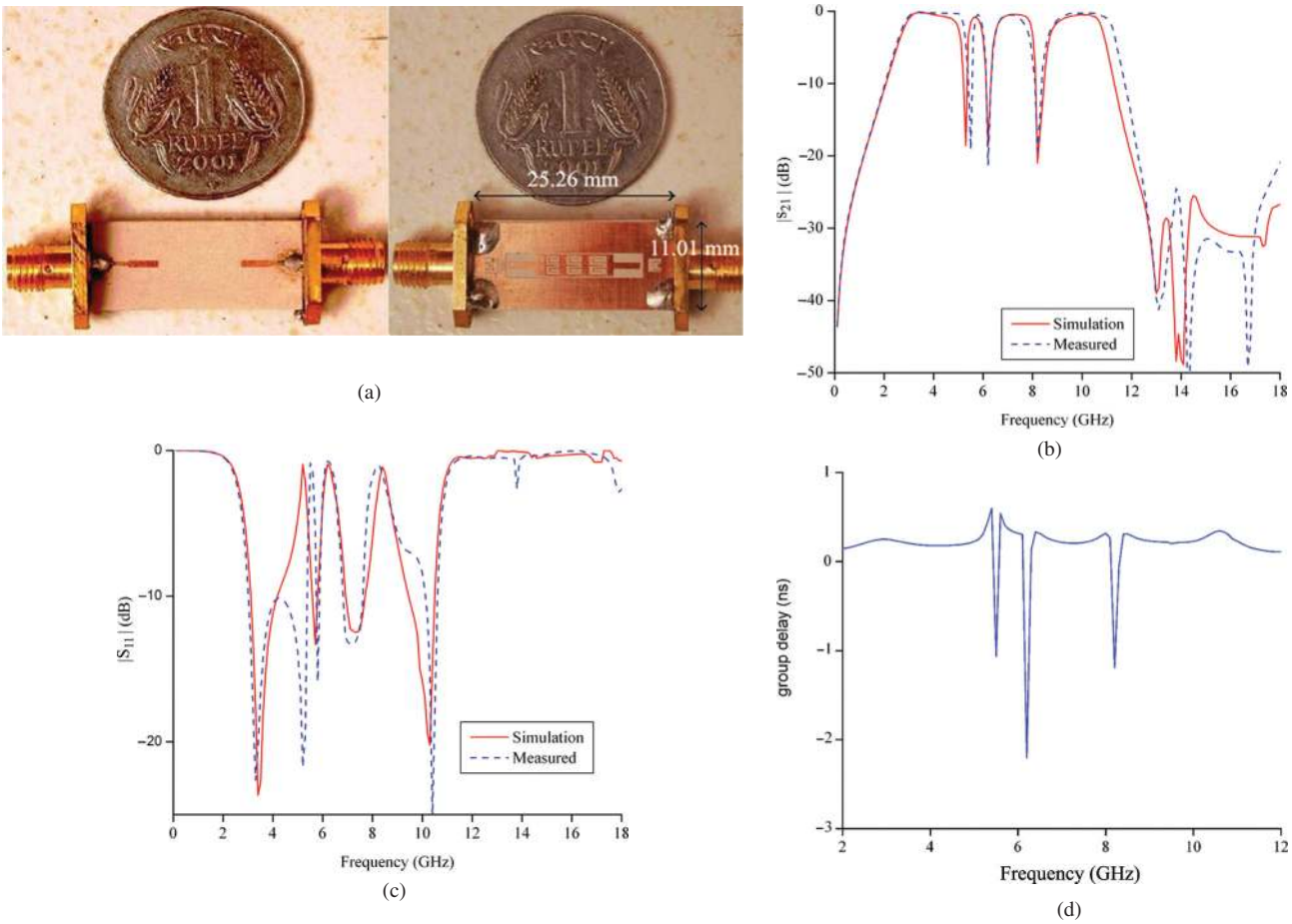

Figure 10: (a) Picture of the fabricated filter. (b) and (c) Measured and simulated S parameters. (d) Group delay.

Table 2: Comparison with some reported UWB filters with notched band.

Ref.	Single notch/ frequency (GHz)/ attenuation (dB)	Dual notch/ frequency (GHz)/ attenuation (dB)	Triple notch/frequency (GHz)/ attenuation (dB)	Stopband width/ depth (dB)	Total circuit dimension (λg @ 6.85 GHz)
[2]	7.0/−20	–	–	Up to 16 GHz/ >−20	0.67 × 0.36
[3]	5.5/−20	–	–	Up to 14.5 GHz/ >−20	>1.5 × 1.18
[4]	–	4.3 and 8.0/−20	–	Up to 14 GHz/ >−15	1.06 × 0.17
[5]	–	5.85 and 8.0/>−15	–	Up to 12.7 GHz/ >−15	1.06 × 0.63
[6]	–	5.2 and 5.8/>−14	–	13/>−18	1.34 × 0.83
[7]	–	–	5.25, 5.85 and 8.0/>−10	Up to 20 GHz/−15	0.96 × 0.63
[8]	–	–	5.25, 5.8 and 8.0/>−15	Up to 17 GHz/−13	1.15 × 0.45
This work	Controllable/ >−15	Controllable/ >−15	5.2, 6.1 and 8.15/>−18	Up to 18 GHz/ >−26	1.53 × 0.67

7 Conclusion

A triple notched band UWB filter with simultaneously extended stopband and flat group delay (variation < 0.25 ns in the passband) is proposed, analysed and implemented. It was shown that by using SDGS and DEU-DGS units, notches (single, double and triple with control over their position, width and number) and simultaneously suppressed stopband can be obtained. An approximate equivalent circuit of the proposed filter is developed. The frequency characteristics of the measured filter are in good agreement with full-wave and circuit simulation.

References

[1] 'Federal Communications Commission, "Revision of Part 15 of the Commission's Rules Regarding Ultra-wideband Transmission Systems', Tech. Rep., April 2002, ET-Docket 98–153, FCC02–4.

[2] S. Pirani, J. Nourinia, and C. Ghobadi, "Band-notched UWB BPF design using parasitic coupled lines," *IEEE Microw. Wireless Compon. Lett.*, vol. 20, pp. 444–456, Aug. 2010.

[3] C. H. Lee, C. I. Hsu, and C. J. Chen, "Band-notched balanced UWB BPF with stepped-impedance slotline multi-mode resonator," *IEEE Microw. Wireless Compon. Lett.*, vol. 22, pp. 182–184, Apr. 2012.

[4] K. Song and Q. Xue, "Compact ultra-wideband (UWB) bandpass filters with multiple notched bands," *IEEE Microw. Wireless Compon. Lett.*, vol. 20, pp. 447–449, Aug. 2010.

[5] F. Wei, Q. Y. Wu, X. W. Shi, and L. Chen, "Compact UWB bandpass filters with dual notched bands based on SCRLH resonator," *IEEE Microw. Wireless Compon. Lett.*, vol. 21, pp. 28–30, Jan. 2011.

[6] B. -W. Liu, Y. -Z. Yin, Y. Yang, S. -H. Jing, and A. -F. Sun, "Compact UWB bandpass filter with two notched bands based on electromagnetic bandgap structures," *Electron. Lett.*, vol. 47, pp. 757–758, June 2011.

[7] F. Wei, W. T. Li, X. W. Shi, and Q. L. Huang, "Compact UWB bandpass filters with triple-notched bands using triple mode stepped impedance resonator," *IEEE Microw. Wireless Compon. Lett.*, vol. 22, pp. 512–514, Oct. 2012.

[8] J. Wang, J. Zhao, and J.-L. Li, "Compact UWB bandpass filter with triple notched bands using parallel U-shaped defected microstrip structure," *Electron. Lett.*, vol. 50, pp. 89–91, Jan. 2014.

[9] H. Wang and L. Zhu, "Ultra-wideband bandpass filter using back to back microstrip to CPW transition structure," *Electron. Lett.*, vol. 41, pp. 1337–1338, Nov. 2005.

[10] S. W. Ting, K. W. Tam, and R. P. Martins, "Miniaturized microstrip lowpass filter with wide SB using double equilateral U-shaped defected ground structure," *IEEE Microw. Wireless Compon. Lett.*, vol. 16, pp. 240–242, May 2006.

[11] D. M. Pozar, *Microwave Engineering*, 2nd ed. New York: John Wiley & Sons, Inc, 1998.

[12] H. Wang, L. Zhu, and W. Menzel, "Ultra-wideband bandpass filter with hybrid microstrip/CPW structure," *IEEE Microw. Wireless Compon. Lett.*, vol. 15, Dec. 2005, pp. 844–846.

[13] H. Liu, Z. Li, X. Sun, S. Kurachi, J. Chen, and T. Yoshimasu, "Theoretical analysis of dispersion characteristics of microstrip lines with defected ground structure," *J. Active Passive Electron. Devices*, vol. 2, pp. 315–322, 2007.

[14] J. S. Hong and B. M. Karyamapudi, "A general circuit model for defected ground structures in planar transmission lines," *IEEE Microw. Wireless Compon. Lett.*, vol. 15, pp. 706–708, Oct. 2005.